Chin. Phys. Lett. **39**, 013401 (2022)

Microwave Induced Ultralong-Range Charge Migration in a Rydberg Atom

Huihui Wang(王慧慧)[1,2], Yuechun Jiao(焦月春)[1,2], Jianming Zhao(赵建明)[1,2*], Liantuan Xiao(肖连团)[1,2], and Suotang Jia(贾锁堂)[1,2]

[1]*State Key Laboratory of Quantum Optics and Quantum Optics Devices, Institute of Laser Spectroscopy, Shanxi University, Taiyuan 030006, China*
[2]*Collaborative Innovation Center of Extreme Optics, Shanxi University, Taiyuan 030006, China*

(Received 13 November 2021; accepted 6 December 2021; published online 29 December 2021)

A microwave induced superposition of the $40S_{1/2}$ and $40P_{1/2}$ states of a Cs atom has been investigated in detail. Ultralong-range charge migration which spans a region more than 200 nm has been discovered. As far as we know, this is the first time to discover charge migration in such a long range. This leads to a large dipole moment which oscillates periodically. The present discovery may stimulate new applications such as quantum simulation of many body physics dominated by periodic interactions. In addition, we find an interesting phenomenon that Cs atoms in the superposition of $40S_{1/2}$ and $40P_{1/2}$ have a much larger blockade radius than those of Cs ($40S_{1/2}$) or Cs ($40P_{1/2}$) atoms.

DOI: 10.1088/0256-307X/39/1/013401

Light induced electron density redistribution has fundamental importance in various processes of physics, chemistry and biology. The redistribution of electron density may lead to the phenomena of charge transfer[1,2] or charge migration.[3–5] Charge migration in molecules typically means ultrafast electron dynamics in a superposition of more than one electronic states. Extensive investigations of laser control of charge migration[5–8] have been preformed due to its important potential applications. For recent surveys in literature on charge migration, one can see Ref. [9]. In particular, attosecond charge migration in $HCCI^+$ has been observed experimentally,[5] which serves as a milestone in the research field of ultrafast charge migration. Charge migration may occur only when more than one electronic states are populated. Consequently, nuclear motions will induce decoherence,[10–12] typically in about 10 fs. A method to fight with decoherence was proposed very recently.[13] Alternatively we can decrease the influence of decoherence of charge migration using systems which naturally have long coherence time. Accordingly charge migration in atoms will have much longer coherence time than in molecules. In particular, the coherence time of a Rydberg atom[14–16] reaches microseconds (μs). Ultralong-range charge migration in a Rydberg atom and the associated extremely large dipole moment is expected to offer a good model system for quantum simulation and manipulation.

Rydberg atoms are highly excited atoms with larger sizes, greater transition dipole moments, and stronger interactions.[17] Accordingly, ultracold Rydberg atoms have emerged as a competitive platform for various applications.[18–21] Rydberg levels can be tuned to Förster resonance by weak electric fields, resulting in strong dipole-dipole interactions and blockade effects.[22–24] The Rydberg blockade effect has been employed to study quantum logic gates,[18] single-photon sources,[19] transistors,[20] and quantum simulation. Large polarizability makes Rydberg atoms quite sensitive to external electric fields. Therefore, Rydberg atoms have also been used for precision measurements of external fields.[25,26] In particular, Rydberg atoms have been widely used for quantum simulation of condensed phase dynamics dominated by dipole interactions,[27,28] Coulomb interactions,[29] strong coupling regime,[30] and so on.[31,32] In this work, we discover ultralong-range charge migration in a Cs Rydberg atom and the resultant fascinating properties. Our results turn out to enhance the competitiveness of Rydberg atoms for state-of-the-art applications.

Specifically, we investigate charge migration in the superposition of the $40S_{1/2}$ and $40P_{1/2}$ states of a Cs atom. Preparation of an initial superposition state $|\psi(t'=0)\rangle = \frac{1}{\sqrt{2}}|40S_{1/2}\rangle + \frac{1}{\sqrt{2}}e^{i\delta}|40P_{1/2}\rangle$ can be carried out by more than one labs in the world with the experimental techniques detailed in the Supplementary Information. The initial state $|\psi(t'=0)\rangle$ will propagate freely, leading to the time-dependent state $|\psi(t')\rangle$ and the electron density $\rho(\boldsymbol{r},t') = \langle\psi(t')|\delta(\boldsymbol{r}-\boldsymbol{r}')|\psi(t')\rangle$. The electron density

*Corresponding author. Email: zhaojm@sxu.edu.cn
© 2022 Chinese Physical Society and IOP Publishing Ltd

$\rho(\boldsymbol{r},t')$ turns out to oscillate around its average value $\langle\rho(\boldsymbol{r})\rangle_T$ periodically with a period $T=\frac{2\pi}{\omega}=15.7$ ps. We only need to focus on the migrating part of the density $\Delta\rho(\boldsymbol{r},t')=\rho(\boldsymbol{r},t')-\langle\rho(\boldsymbol{r})\rangle_T$. For convenience, we define the starting time $t=0$ for observing electron density as $t=t'-\frac{\delta}{\omega}$. Then, $\Delta\rho(\boldsymbol{r},t)$ will have largest amplitude at $t=0$. Large amplitude charge migration mainly occurs along the polarization of the field, which is defined as the z-axis. Consequently it is convenient to focus on the one-dimensional reduced density $\Delta\rho(z,t)$ along z-axis, which can be obtained by integrating $\Delta\rho(x,y,z,t)$ over x and y. Accordingly the propagation of $\Delta\rho(z,t)$ is shown in Fig. 1 for one period T.

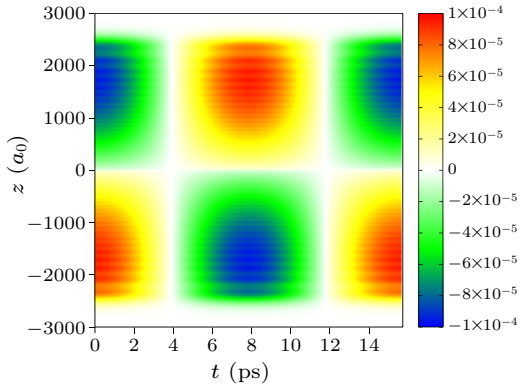

Fig. 1. The migrating part of the one-dimensional reduced electron density $\Delta\rho(z,t)$ in units of a_0^{-1}.

In the following, we use charge to represent negative charge contributed by electron distribution. Charge migration along z-axis can be clearly identified in Fig. 1. In the beginning stage, more density is accumulated in the region of $z<0$. Consequently there is charge migration from $z<0$ to $z>0$, namely along the positive direction of z-axis. At $t=\frac{T}{4}$ the density $\Delta\rho(z,t)$ is exactly zero for all z. Therefore, the density distribution at $t=\frac{T}{4}$ is just the average one $\langle\rho(z)\rangle_T$. The charge keeps migrating from $z<0$ to $z>0$ until $t=\frac{T}{2}$. Then more density is accumulated in the region of $z>0$. Consequently, the direction of charge migration changes for the next half period. The charge is migrating from $z>0$ to $z<0$ for $\frac{T}{2}<t<T$.

On closer inspection of $\Delta\rho(z,t)$, the maximum amplitudes of the density oscillation are located around $\pm1700a_0$. Many small oscillations of $\Delta\rho(z,t)$ can be found along z, due to the oscillation nature of Rydberg wavefunctions. More details of the oscillation characteristics can be unraveled by a two-dimensional representation of $\Delta\rho(\boldsymbol{r},t)$. Accordingly the complete information of $\Delta\rho(\boldsymbol{r},t)$ is provided in the Supplementary Information in terms of the cylindrical coordinates. Charge migration is noticeable in the region $-2500a_0<z<2500a_0$, which spans more than 200 nm. The order of magnitude for the migration speed can be estimated to be $2\times200\,\text{nm}/15.72\,\text{ps}\approx25\,\text{km/s}$, while the corresponding order of magnitude for the case of $HCCI^+$ is 2×0.25 nm/1.85 fs $\approx$ 270 km/s.[5,33] The latter is one order of magnitude larger, because the kinetic energy of valence electrons are much larger than that of Rydberg electrons.

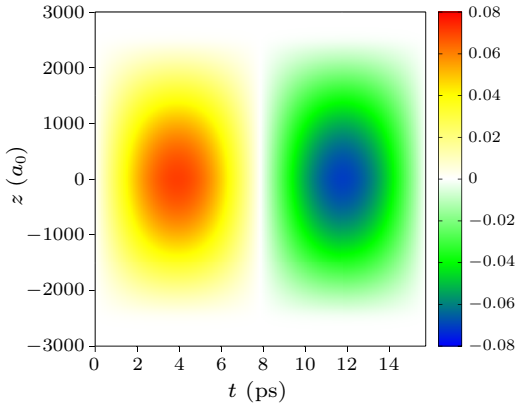

Fig. 2. The electron flux $F_z(z,t)$ along z-axis in units of ps^{-1}.

A more convenient tool to study charge migration is the electron flux density or flux.[34–36] For one-dimensional charge migration, the electron flux $F_z(z,t)$ along z-axis is sufficient.[12] The electron flux $F_z(z,t)$ can be obtained either by integrating the flux density in each plane perpendicular to z-axis or from the continuity equation. The corresponding electron flux $F_z(z,t)$ is shown in Fig. 2 for one period T. Positive (or negative) values of $F_z(z,t)$ means charge migration along the positive (or negative) direction of z-axis. Apparently there is unidirectional charge migration along the positive direction of z-axis for the first half period $0<t<\frac{T}{2}$. The electron flux reaches its maximum at $t=\frac{T}{4}$ and then decreases to zero at $t=\frac{T}{2}$. The direction of charge migration changes to the negative direction of z-axis for the next half period $\frac{T}{2}<t<T$. For any given time $t\neq0,\frac{T}{2},T$, the electron flux $F_z(z,t)$ has its maximum amplitudes at $z=0$. This is just because all the electron density migrating from $z<0$ to $z>0$ or the reverse must pass the position $z=0$. This fact leads to a natural way of evaluating the total migrating charge ΔQ_m, which migrates between the two regions $z<0$ and $z>0$. The total migrating charge ΔQ_m can be obtained by integrating $F_z(z,t)$ at $z=0$ for the first half period. More intuitively, an equivalently way to obtain ΔQ_m is to compare $\Delta\rho(z,t)$ at different times in the $z<0$ or $z>0$ regions. In the Supplementary Information, four equivalent calculations all lead to the migrating charge $\Delta Q_m=-0.35e$. The total migrating charge ΔQ_m is similar to the value of the corresponding migrating charge in molecules.[12,37]

The amplitude and range of charge migration are directly related to the value of the system dipole mo-

ment. The present superposition of the $40S_{1/2}$ and $40P_{1/2}$ states leads to an extremely large dipole moment even when the external field is exactly zero. At the time $t = 0$, the dipole moment is 1305.7 Debye. The dipole moment changes to -1305.7 Debye at $t = \frac{T}{2}$. When all the external fields are switched off, the system dipole moment oscillates between 1305.7 and -1305.7 Debye. This leads to large dipole-dipole interactions between two such atoms. It is worth noting that the dipole-dipole interaction has a distance dependence of $\frac{1}{R^3}$. However, the Van der Waals interaction between two normal Rydberg atoms has a distance dependence of $\frac{1}{R^6}$. Consequently the interaction between two Rydberg atoms which are both in the present superposition of the $40S_{1/2}$ and $40P_{1/2}$ states will be much larger than the interaction between two $40S_{1/2}$ (or $40P_{1/2}$) Rydberg atoms, provided that the distance is long enough. For example, if the distance between two Cs atoms is 5 μm (which corresponds to typical Rydberg blockade radius), the maximum interaction is as large as 4.1 MHz for the present superposition states. The interaction for two Cs $40S_{1/2}$ atoms at the same distance is only 0.04 MHz, and even smaller for the case of $40P_{1/2}$. This implies an ever larger blockade radius if we want to prepare ensembles of Rydberg atoms in the present superposition state rather than in the $40S_{1/2}$ (or $40P_{1/2}$) state.

Experimental realization of the system is feasible. Here we design an experiment to prepare the superposition state employing well-developed techniques for Rydberg atom, see the Supplementary Information for more details. Ultracold cesium atoms can be first trapped in a magneto-optical trap (MOT) then loaded into a tightly focused optical tweeze to prepare a single atom. The MOT temperature can be decreased to a few μK. The Rydberg $|40S_{1/2}(m_J = 1/2)\rangle$ state will be prepared from the $|6S_{1/2}(F = 4, m_F = 4)\rangle$ state with a two-photon scheme using an 852 nm laser with the σ^+ polarization and a 510 nm laser with the σ^- polarization via the $|6P_{3/2}(F' = 5, m_F = 5)\rangle$ intermediate state. To prepare the state of interest, a 63.6 GHz microwave field will be employed to couple the $40S_{1/2}$ and $40P_{1/2}$ states. The microwave field is linearly polarized along z-axis so that the quantum number $m_J = 1/2$ is unchanged during the transition. When the microwave field is switched off, the population of the $40S_{1/2}$ and $40P_{1/2}$ states will be $\cos^2\gamma$ and $\sin^2\gamma$, respectively. Thus the initial superposition state for charge migration is $|\psi(t' = 0)\rangle = \cos\gamma\,|40S_{1/2}\rangle + \sin\gamma e^{i\delta}\,|40P_{1/2}\rangle$ with a phase difference δ undetermined. Here $m_J = 1/2$ is omitted. The relative error of γ is only a few percent, mainly due to the time for switching on/off of the microwave field. However, the error of γ will only lead to a different initial state which gives the same charge migration except for a different amplitude.

A linearly polarized microwave field induced partial transition between two Rydberg states can lead to ultralong-range charge migration. As far as we know, this is the first time to discover charge migration through a region exceeding 200 nm. In addition, it is straight forward to increase the range of charge migration to micrometers, e.g., by preparing a superposition of the $80S_{1/2}$ and $80P_{1/2}$ states instead of the present superposition of the $40S_{1/2}$ and $40P_{1/2}$ states. The phenomenon of charge migration may be experimentally confirmed in terms of high-contrast time-domain Ramsey interferometry.[32,38] The extremely large dipole moments mediated by ultralong-range charge migration result in large dipole-dipole interactions between atoms in the same superposition state. The large dipole-dipole interactions may be experimentally detected.[28,31] Compared to Cs Rydberg atoms of the $40S_{1/2}$ or $40P_{1/2}$, the interactions between atoms in the superposition of $40S_{1/2}$ and $40P_{1/2}$ states are about two orders of magnitude larger for distances of typical Rydberg blockade radius. Consequently there exists an even larger blockade radius than typical Rydberg blockade radius. This even larger blockade radius may be measured based on the well-developed experimental techniques for the Rydberg blockade effect. For an ensemble of atoms prepared by the same microwave field, all the dipole moments will oscillate concertedly. If they are loaded in a one-dimensional lattice, the interactions will be periodic. This opens the door to a new type of quantum simulation, for a system dominated by periodic interactions.

We would like to express our gratitude to Professor Jörn Manz (Berlin) for stimulating discussions and careful reading of the manuscript. This work was supported by the National Key Research and Development Program of China (Grant No. 2017YFA0304203), the Program for Changjiang Scholars and Innovative Research Team in University of Ministry of Education of China (Grant No. IRT_17R70), the National Natural Science Foundation of China (Grant No. 11904215), the 111 Project (Grant No. D18001), the Fund for Shanxi "1331 Project", and the Hundred Talent Program of Shanxi Province.

References

[1] Marcus R A 1956 *J. Chem. Phys.* **24** 966
[2] May V and Kühn O 2011 *Charge and Energy Transfer Dynamics in Molecular Systems* (New York: WILEY-VCH Verlag)
[3] Weinkauf R, Schanen P, Metsala A, Schlag E W, Bürgle M and Kessler H 1996 *J. Phys. Chem.* **100** 18567
[4] Cederbaum L S and Zobeley J 1999 *Chem. Phys. Lett.* **307** 205
[5] Kraus P M, Mignolet B, Baykusheva D, Rupenyan A, Horny

L, Penka E F, Grassi G, Tolstikhin O I, Schneider J, Jensen F, Madsen L B, Bandrauk A D, Remacle F and Wörner H J 2015 *Science* **350** 790
[6] Barth I and Manz J 2006 *Angew. Chem. Int. Ed.* **45** 2962
[7] Jia D, Manz J, Paulus B, Pohl V, Tremblay J C and Yang Y 2017 *Chem. Phys.* **482** 146
[8] Li H, Mignolet B, Wachter G, Skruszewicz S, Zherebtsov S, Süßmann F, Kessel A, Trushin S A, Kling N G, Kübel M, Ahn B, Kim D, Ben-Itzhak I, Cocke C L, Fennel T, Tiggesbäumker J, Meiwes-Broer K H, Lemell C, Burgdörfer J, Levine R D, Remacle F and Kling M F 2015 *Phys. Rev. Lett.* **114** 123004
[9] Wörner H J, Arrell C A, Banerji N, Cannizzo A, Chergui M, Das A K, Hamm P, Keller U, Kraus P M, Liberatore E, Lopez-Tarifa P, Lucchini M, Meuwly M, Milne C, Moser J E, Rothlisberger U, Smolentsev G, Teuscher J, van Bokhoven and Wenger O 2017 *Struct. Dyn.* **4** 061508
[10] Bandrauk A D, Chelkowski S, Corkum P B, Manz J and Yudin G L 2009 *J. Phys. B* **42** 134001
[11] Despré V, Golubev N V and Kuleff A I 2018 *Phys. Rev. Lett.* **121** 203002
[12] Jia D, Manz J and Yang Y 2019 *J. Phys. Chem. Lett.* **10** 4273
[13] Jia D, Manz J and Yang Y 2019 *J. Chem. Phys.* **151** 244306
[14] Dudin Y O and Kuzmich A 2012 *Science* **336** 887
[15] Hermann-Avigliano C, Teixeira R C, Nguyen T L, Cantat-Moltrecht T, Nogues G, Dotsenko I, Gleyzes S, Raimond J M, Haroche S and Brune M 2014 *Phys. Rev. A* **90** 040502
[16] Lampen J, H N H, Li L, Berman P R and Kuzmich A 2018 *Phys. Rev. A* **98** 033411
[17] Gallagher T F 1994 *Rydberg Atoms* (New York: Cambridge University Press)
[18] Urban E, Johnson T A, Henage T, Isenhower L, Yavuz D D, Walker T G and Saffman M 2009 *Nat. Phys.* **5** 110
[19] Peyronel T, Firstenberg O, Liang Q Y, Hofferberth S, Gorshkov A V, Pohl T, Lukin M D and Vuletić V 2012 *Nature* **488** 57
[20] Tiarks D, Baur S, Schneider K, Dürr S and Rempe G 2014 *Phys. Rev. Lett.* **113** 053602
[21] Moore K R, Anderson S E and Raithel G 2015 *Nat. Commun.* **6** 6090
[22] Vogt T, Viteau M, Zhao J, Chotia A, Comparat D and Pillet P 2006 *Phys. Rev. Lett.* **97** 083003
[23] Comparat D and Pillet P 2010 *J. Opt. Soc. Am. B* **6** A208
[24] Paredes-Barato D and Adams C S 2014 *Phys. Rev. Lett.* **112** 040501
[25] Sedlacek J A, Schwettmann A, Kübler H, Löw R, Pfau T and Shaffer J P 2012 *Nat. Phys.* **8** 819
[26] Jing M, Hu Y, Ma J, Zhang H, Zhang L, Xiao L and Jia S 2020 *Nat. Phys.* **16** 911
[27] Günter G, Schempp H, Robert-de S V M, Gavryusev V, Helmrich S, Hofmann C S, Whitlock S and Weidemüller M 2013 *Science* **342** 954
[28] Orioli A P, Signoles A, Wildhagen H, Günter G, Berges J, Whitlock S and Weidemüller M 2018 *Phys. Rev. Lett.* **120** 063601
[29] Mizoguchi M, Zhang Y, Kunimi M, Tanaka A, Takeda S, Takei N, Bharti V, Koyasu K, Kishimoto T, Jaksch D, A G A, Kiffner M, Masella G, Pupillo G, Weidemüller M and Ohmori K 2020 *Phys. Rev. Lett.* **124** 253201
[30] Sheng J, Chao Y and Shaffer J P 2016 *Phys. Rev. Lett.* **117** 103201
[31] Thaicharoen N, Gonçalves L F and Raithel G 2016 *Phys. Rev. Lett.* **116** 213002
[32] Takei N, Sommer C, Genes C, Pupillo G, Goto H, Koyasu K, Chiba H, Weidemüller M and Ohmori K 2016 *Nat. Commun.* **7** 13449
[33] Ding H, Jia D, Manz J and Yang Y 2017 *Mol. Phys.* **115** 1813
[34] Manz J, Pérez-Torres J F and Yang Y 2013 *Phys. Rev. Lett.* **111** 153004
[35] Manz J, Pérez-Torres J F and Yang Y 2014 *J. Phys. Chem. A* **118** 8411
[36] Jia D, Manz J and Yang Y 2018 *J. Chem. Phys.* **148** 041101
[37] Jia D, Manz J and Yang Y 2017 *J. Mod. Opt.* **64** 960
[38] Liu C, Manz J, Ohmori K, Sommer C, Takei N, Tremblay J C and Zhang Y 2018 *Phys. Rev. Lett.* **121** 173201

Supplementary Information: Microwave-Induced Ultralong-Range Charge Migration in a Rydberg Atom

Huihui Wang(王慧慧)[1,2], Yuechun Jiao(焦月春)[1,2], Jianming Zhao(赵建明)[1,2*],
Liantuan Xiao(肖连团)[1,2], Suotang Jia(贾锁堂)[1,2]

[1]*State Key Laboratory of Quantum Optics and Quantum Optics Devices, Institute of Laser Spectroscopy, Shanxi University, Taiyuan, 030006, China;*

[2]*Collaborative Innovation Center of Extreme Optics, Shanxi University, Taiyuan, 030006, China*

I. PROPAGATION OF THE ELECTRON DENSITY

The Rydberg state $40S_{1/2}$ means a state with principle quantum number $n = 40$, quantum numbers for orbital angular momentum $l = 0$ and total angular momentum $J = 1/2$, respectively. Through this work we focus on Cs Rydberg atoms. The two involved states $40S_{1/2}$ and $40P_{1/2}$ with the same z-component of J ($m_J = 1/2$) will be written as $|40S_{\frac{1}{2},\frac{1}{2}}\rangle$ and $|40P_{\frac{1}{2},\frac{1}{2}}\rangle$, respectively. By solving the time-dependent Schrödinger equation we obtain the time propagation of the initial state $|\psi(t'=0)\rangle = \cos\gamma\,|40S_{1/2}\rangle + \sin\gamma e^{i\delta}\,|40P_{1/2}\rangle$ as

$$|\psi(t')\rangle = \cos\gamma e^{-iE_{40S_{1/2}}t'/\hbar}\,|40S_{\frac{1}{2},\frac{1}{2}}\rangle + \sin\gamma e^{i\delta - iE_{40P_{1/2}}t'/\hbar}\,|40P_{\frac{1}{2},\frac{1}{2}}\rangle\,, \tag{1}$$

where $E_{40S_{1/2}}$ and $E_{40P_{1/2}}$ are the eigenenergies of the two egenstates $|40S_{\frac{1}{2},\frac{1}{2}}\rangle$ and $|40P_{\frac{1}{2},\frac{1}{2}}\rangle$, respectively. In the representation of electron position $\mathbf{r}'$ and electron spin ξ', the wavefunction is $\psi(\mathbf{r}',\xi',t') = \langle \mathbf{r}',\xi'|\psi(t')\rangle$. The eigenfunctions of the two involved states can be factorized as

$$\begin{aligned}\langle \mathbf{r}',\xi'|40S_{\frac{1}{2},\frac{1}{2}}\rangle &= R_{40S_{1/2}}(r')\chi_{0\frac{1}{2}\frac{1}{2}}(\xi',\theta',\varphi'),\\ \langle \mathbf{r}',\xi'|40P_{\frac{1}{2},\frac{1}{2}}\rangle &= R_{40P_{1/2}}(r')\chi_{1\frac{1}{2}\frac{1}{2}}(\xi',\theta',\varphi').\end{aligned} \tag{2}$$

Here $R_{40S_{1/2}}(r)$ and $R_{40P_{1/2}}(r)$ are the corresponding radial wavefunctions. The radial wavefunction $R_{nlJ}(r)$ is obtained by the Alkali Rydberg Calculator (ARC) package codes as detailed in ref [1]. The effective one-electron potential includes the spin-orbit interaction term $\frac{\mathbf{L}\cdot\mathbf{S}}{137^2\times 2r^3}$ as implemented in the ARC codes. Consequently the effective potential and the radial wavefunctions depend on the quantum number J. Accordingly the radial probability densities $P(r) = r^2R^2_{nlJ}(r)$ of the $40S_{1/2}$ and $40P_{1/2}$ states are shown in Fig. S1.

The functions for electron spin ξ' and the two angles (θ',φ') are

$$\begin{aligned}\chi_{0\frac{1}{2}\frac{1}{2}}(\xi',\theta',\varphi') &= \alpha(\xi')Y_{00}(\theta',\varphi'),\\ \chi_{1\frac{1}{2}\frac{1}{2}}(\xi',\theta',\varphi') &= -\sqrt{\frac{1}{3}}\alpha(\xi')Y_{10}(\theta',\varphi') + \sqrt{\frac{2}{3}}\beta(\xi')Y_{11}(\theta',\varphi').\end{aligned} \tag{3}$$

Here $\alpha(\xi')$ and $\beta(\xi')$ are the spin wavefunctions for the states with spin-up and spin-down, respectively. And $Y_{lm}(\theta',\varphi')$ is the spherical harmonics. To simplify the notations, $R_{40S_{1/2}}(r)$ and $R_{40P_{1/2}}(r)$ will be written as $R_{40S}(r)$ and $R_{40P}(r)$, respectively.

The expression of the system wavefunction $\psi(\mathbf{r}',\xi',t') = \langle \mathbf{r}',\xi'|\psi(t')\rangle$ can be obtained from eqs. (1-3). The corresponding electron density $\rho(\mathbf{r},t')$ can be obtained by evaluating the mean value of the density operator

*Electronic address: zhaojm@sxu.edu.cn

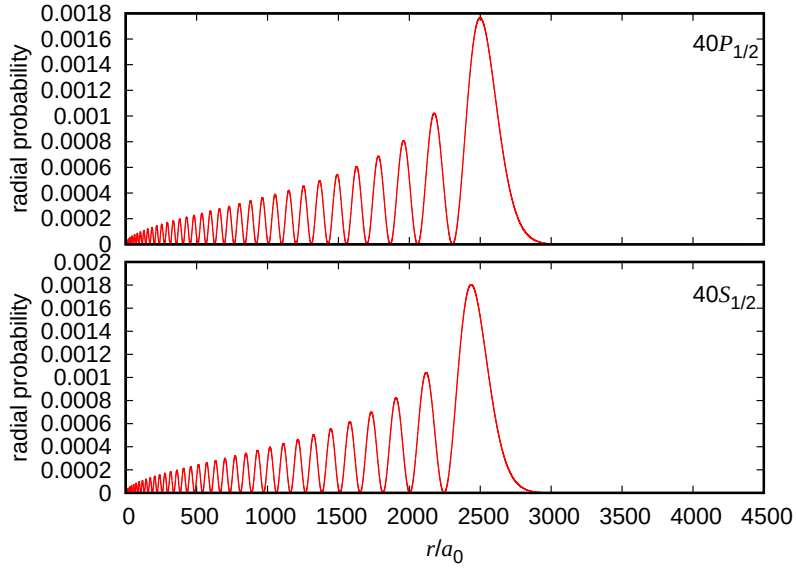

Figure S1: The radial probability density $P(r) = r^2 R_{nlJ}^2(r)$.

$$\begin{aligned}\rho(\mathbf{r},t') &= \langle\psi(t')|\delta(\mathbf{r}-\mathbf{r}')|\psi(t')\rangle \\ &\equiv \int \psi^*(\mathbf{r}',\xi',t')\delta(\mathbf{r}-\mathbf{r}')\psi(\mathbf{r}',\xi',t')d\mathbf{r}'d\xi' \\ &= \cos^2\gamma R_{40S}^2 Y_{00}^2 + \sin^2\gamma R_{40P}^2(\frac{1}{3}Y_{10}^2 + \frac{2}{3}Y_{11}^2) \\ &- \sqrt{\frac{1}{3}}\sin 2\gamma\cos(\delta-\omega t')R_{40S}R_{40P}Y_{00}Y_{10},\end{aligned} \tag{4}$$

where $\omega = \frac{E_{40P_{1/2}} - E_{40S_{1/2}}}{\hbar} = 2\pi \times 63.6$ GHz.

The phase difference δ only defines the time reference. Observing $\rho(\mathbf{r},t')$ starting from different time will not change the essence of the charge migration phenomenon. For convenience we define $t' = \frac{\delta}{\omega}$ as the starting time for observing the density, namely a new time $t = t' - \frac{\delta}{\omega}$. The migrating part of the density is

$$\begin{aligned}\Delta\rho(\mathbf{r},t) &= \rho(\mathbf{r},t) - \langle\rho(\mathbf{r})\rangle_T \\ &= -\sqrt{\frac{1}{3}}\sin 2\gamma\cos(\omega t)R_{40S}R_{40P}Y_{00}Y_{10},\end{aligned} \tag{5}$$

where $\langle\rho(\mathbf{r})\rangle_T$ is the average density in one period $T = \frac{1}{63.6\text{ GHz}} = 15.7$ ps. Apparently $\langle\rho(\mathbf{r})\rangle_T$ is just the sum of the time-independent terms in Eq. (4).

Since the microwave is polarized along z-axis, the migrating part of the density $\Delta\rho(\mathbf{r},t)$ has cylindrical symmetry. It is then convenient to use the cylindrical coordinates (z,u,φ). The relations between the cylindrical coordinates, the spherical coordinates (r,θ,φ), and the cartesian coordinates (x,y,z) are

$$\begin{cases} z = r\cos\theta \\ u = r\sin\theta \\ \varphi = \varphi \end{cases}, \quad \begin{cases} x = u\cos\varphi \\ y = u\sin\varphi \\ z = z \end{cases}. \tag{6}$$

The migrating part of the density $\Delta\rho$ does not depend on φ. Figures S2a and S2b show the details of $\Delta\rho(z,u,t=0)$ and $\Delta\rho(z,u,t=\frac{T}{2})$, respectively. The net charge migration is apparently from $z<0$ to $z>0$ for $0<t<\frac{T}{2}$.

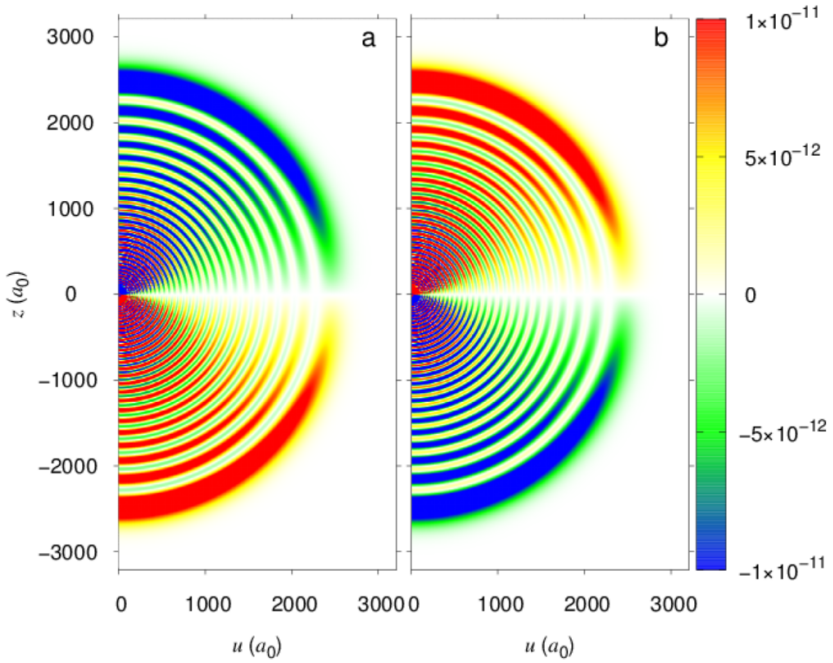

Figure S2: The migrating part of the density $\Delta\rho(z,u,\varphi,t)$ at a given time t for arbitrary φ in the cylindrical coordinates (z,u,φ). The unit of $\Delta\rho$ is a_0^{-3}. Panels A and B are for $t=0$ and $t=\frac{T}{2}$, respectively.

However there are also some small regions in which the charge migrates in the opposite direction. This is a consequence of the large number of nodes of the radial wavefunctions.

In the following we focus on the one-dimensional electron density $\Delta\rho(z,t)$ along z-axis

$$\Delta\rho(z,t)=\int_{-\infty}^{\infty}\int_{-\infty}^{\infty}\Delta\rho(\mathbf{r},t)dxdy=2\pi\int_{0}^{\infty}\Delta\rho(z,u,t)udu. \tag{7}$$

In the numerical calculations, we first get $\Delta\rho(z,u,t)$ in the cylindrical coordinates. Then we obtain $\Delta\rho(z,t)$ by integrating $\Delta\rho(z,u,t)$ over u. The one-dimensional densities $\Delta\rho(z,t)$ at different times are shown in Fig. S3.

II. THE ELECTRON FLUX DENSITY AND FLUX

The flux density can be obtained as the mean value of the flux operator

$$\begin{aligned}\mathbf{j}(\mathbf{r},t)&=\langle\psi(t)|\frac{\mathbf{P}}{2m}\delta(\mathbf{r}-\mathbf{r}')+\delta(\mathbf{r}-\mathbf{r}')\frac{\mathbf{P}}{2m}|\psi(t)\rangle\\&=\frac{\hbar}{4\sqrt{3\pi}m}\sin(2\gamma)\sin(\omega t)\\&\times[R_{40S}\nabla(R_{40P}Y_{10})-R_{40P}Y_{10}\nabla R_{40S}],\end{aligned} \tag{8}$$

where $\mathbf{P}=-i\hbar\nabla$ is the momentum operator. In the spherical coordinates, the flux density is

$$\mathbf{j}(\mathbf{r},t)=\hat{\mathbf{e}}_r j_r(\mathbf{r},t)+\hat{\mathbf{e}}_\theta j_\theta(\mathbf{r},t)+\hat{\mathbf{e}}_\varphi j_\varphi(\mathbf{r},t). \tag{9}$$

Apparently we have $j_\varphi(\mathbf{r},t)=0$. The other two components are

$$\begin{aligned}j_r(\mathbf{r},t)&=\frac{\hbar}{8\pi m}\sin(2\gamma)\sin(\omega t)\cos\theta[R_{40S}\frac{dR_{40P}}{dr}-R_{40P}\frac{dR_{40S}}{dr}],\\j_\theta(\mathbf{r},t)&=-\frac{\hbar}{8\pi m}\sin(2\gamma)\sin(\omega t)\frac{1}{r}R_{40S}R_{40P}\sin\theta.\end{aligned} \tag{10}$$

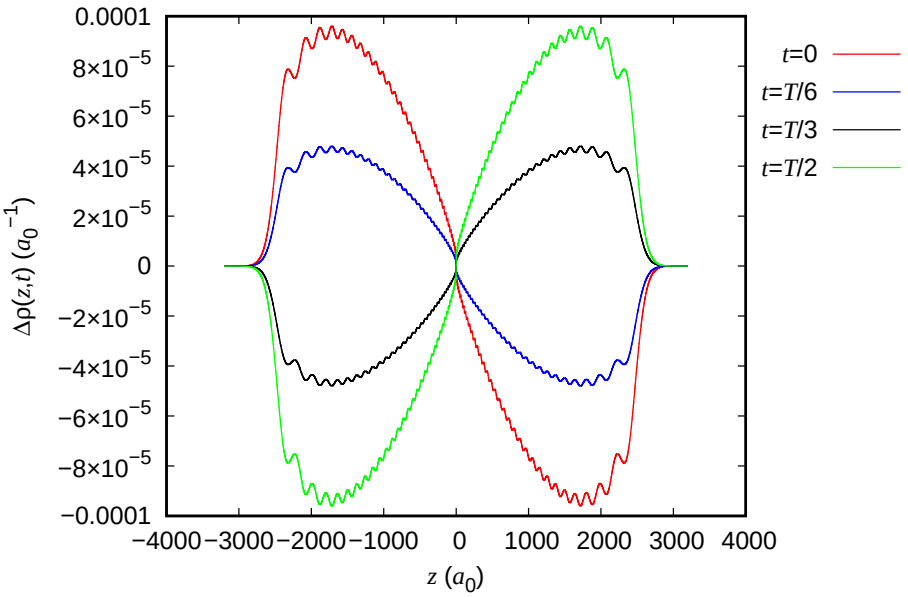

Figure S3: The migrating part of the density $\Delta\rho(z,t)$ at different time in units of a_0^{-1}.

The electron flux along z-axis F_z can be obtained by

$$\begin{aligned} F_z(z,t) &= \int_{-\infty}^{\infty}\int_{-\infty}^{\infty} \mathbf{j}(\mathbf{r},t)\cdot\hat{\mathbf{e}}_z dxdy \\ &= \frac{\hbar}{8\pi m}\sin(2\gamma)\sin(\omega t)\int_{-\infty}^{\infty}\int_{-\infty}^{\infty}[\cos^2\theta R_{40S}\frac{dR_{40P}}{dr} \\ &- \cos^2\theta R_{40P}\frac{dR_{40S}}{dr} + \frac{1}{r}\sin^2\theta R_{40S}R_{40P}]dxdy. \end{aligned} \tag{11}$$

In principle we can carry out the above two-fold integration to get $F_z(z,t)$. However there is an alternative way to get the flux $F_z(z,t)$ according to the one-dimensional continuity equation

$$\frac{\partial F_z(z,t)}{\partial z} + \frac{\partial \rho(z,t)}{\partial t} = 0. \tag{12}$$

Accordingly the flux $F_z(z,t)$ can be evaluated by

$$F_z(z,t) = -\int_{-\infty}^{z}\frac{\partial \Delta\rho(z',t)}{\partial t}dz'. \tag{13}$$

Since we already have $\Delta\rho(z,t)$ at hand, the electron flux $F_z(z,t)$ is obtained by Eq. (13).

III. THE DIPOLE MOMENT AND THE MIGRATING CHARGE

The dipole moment of the system can be obtained by evaluating the mean value of the dipole operator

$$\boldsymbol{\mu}(t) = -\langle\psi(t)|e\mathbf{r}|\psi(t)\rangle\,. \tag{14}$$

The only nonzero component of $\boldsymbol{\mu}(t)$ is

$$\mu_z(t) = -\langle\psi(t)|ez|\psi(t)\rangle = -e\int_{-\infty}^{+\infty} z\Delta\rho(z,t)dz. \tag{15}$$

By numerical integration of eq.(15) we obtain $\mu_z(t) = \mu_z^{max}\cos(\omega t)$ with $\mu_z^{max} = 513.7\ ea_0 = 1305.7$ Debye.

The total migrating charge ΔQ_m can be obtained in terms of either the flux $F_z(z,t)$ or the density $\Delta\rho(z,t)$. The following four equivalent expressions all get the total charge which migrates from $z<0$ to $z>0$ (or the reverse) in a half period $\frac{T}{2}$:

$$\begin{aligned}\Delta Q_m &= -e\int_0^{\frac{T}{2}} F_z(z=0,t)dt \\ &= e\int_{\frac{T}{2}}^{T} F_z(z=0,t)dt \\ &= -e\int_{-\infty}^{0}[\Delta\rho(z,t=0)-\Delta\rho(z,t=\frac{T}{2})]dz \\ &= -e\int_{0}^{+\infty}[\Delta\rho(z,t=\frac{T}{2})-\Delta\rho(z,t=0)]dz \\ &= -0.35e.\end{aligned} \tag{16}$$

IV. DETAILS FOR FEASIBLE EXPERIMENTAL REALIZATION

For the experiment, cesium atoms will be trapped in a magneto-optical trap (MOT) with a temperature of about 100 μK using laser cooling and trap technique. The MOT temperature can be further decreased to a few μK by an optical molasses and evaporation cooling technique. The ultracold Cs atoms are then loaded into a tightly focused optical tweeze to prepare a single atom and then optically pumped to the $|6S_{1/2}(F=4,m_F=4)\rangle$ Zeeman level with a circularly polarized laser. Rydberg excitation of the $|40S_{1/2}(m_J=1/2)\rangle$ state can be realized with a two-photon scheme as shown in Fig. S4a. Firstly a 852 nm laser with the σ^+ polarization drives the $|6S_{1/2}(F=4,m_F=4\rangle)$ to $|6P_{3/2}(F'=5,m_F=5)\rangle$ transition. Then a 510 nm laser with the σ^- polarization excites the $|6P_{3/2}(F'=5,m_F=5)\rangle$ state to the $|40S_{1/2}(m_J=1/2)\rangle$ state.

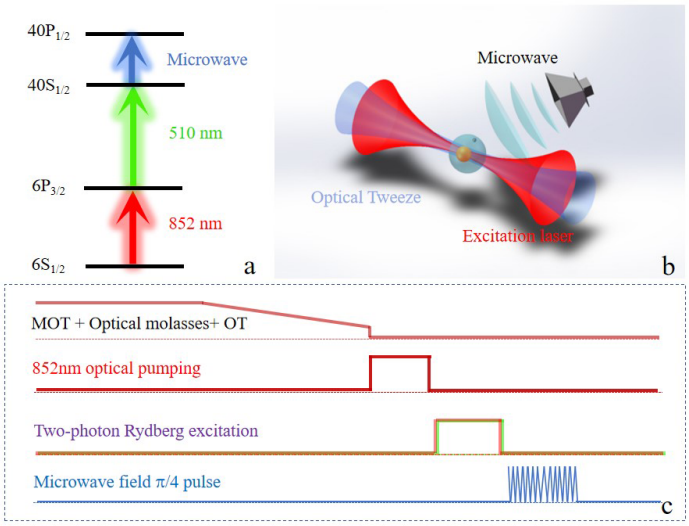

Figure S4: The scheme for the preparation of the initial state $|\psi(t'=0)\rangle$. a. Two-photon excitation to the Rydberg state $40S_{1/2}$ and partial transition from $40S_{1/2}$ to $40P_{1/2}$ by a microwave pulse. b. The experimental setup. The cesium atoms are first trapped in a MOT (not shown in here), then loaded into a optical tweeze (OT). c. The time sequence for loading and cooling, optical pumping, Rydberg excitation, and microwave transition.

After that, a linearly polarized (z-polarization) 63.6-GHz microwave field can be applied to couple the $|40S_{\frac{1}{2},\frac{1}{2}}\rangle$ and $|40P_{\frac{1}{2},\frac{1}{2}}\rangle$ states, which produces a superposition state of $|40S_{\frac{1}{2},\frac{1}{2}}\rangle$ and $|40P_{\frac{1}{2},\frac{1}{2}}\rangle$. The interaction

between the microwave and a Cs atom is $-\boldsymbol{\mu}^{\mathrm{T}} \cdot \mathbf{E}$, where $\boldsymbol{\mu}^{\mathrm{T}}$ is the transition dipole moment and $\mathbf{E}$ is the amplitude of the microwave field. Since the field is z-polarized, we only need the z-component μ_z^{T}, which is -1305.2 Debye. By selecting appropriate microwave pulse parameters, the initial state can be prepared as $|\psi(t'=0)\rangle = \cos\gamma\,|40S_{\frac{1}{2},\frac{1}{2}}\rangle + \sin\gamma e^{i\delta}\,|40P_{\frac{1}{2},\frac{1}{2}}\rangle$. The details of the experimental setup and the time sequence of the applied external fields are shown in Figs. S4b and S4c, respectively. For the experimental condition with a field strength of 1.0 mV/cm and a pulse duration of 0.38 μs, $\gamma = \frac{\pi}{4}$ is reached which corresponds to equal population of the $40S_{1/2}$ and $40P_{1/2}$ states. This can be verified by the state-selective field ionization technique. The phase difference δ can not be determined. However the information we obtained is sufficient to unravel the essence of charge migration. Note the phenomenon of ultralong-range charge migration is more or less robust for different parameters δ and γ.

---

[1] Šibalić N, Pritchard J D, Weatherill K J and Adams C S 2017 *Comput. Phys. Commun.* **220** 319